Available online at www.sciencedirect.com
SCIENCE DIRECT®
Experimental Thermal and Fluid Science 30 (2005) 49–57
Experimental Thermal and Fluid Science
www.elsevier.com/locate/etfs

A look at three measurement techniques for bubble size determination

A. Vazquez [a], R.M. Sanchez [a], E. Salinas-Rodríguez [a], A. Soria [a,*], R. Manasseh [b]

[a] Group of Dispersed Multiphase Systems, Universidad Autónoma Metropolitana—Iztapalapa, Dep. I.P.H., Av. San Rafael Atlixco No. 186, Col. Vicentina C.P. 09340, Mexico, DF

[b] Energy and ThermoFluids Engineering, CSIRO Manufacturing and Infrastructure Technology, P.O. Box 56, Highett, VIC 3190, Melbourne, Australia

Received 1 October 2004; accepted 13 March 2005

Abstract

Three methods for measuring the volume and the equivalent radius of air bubbles at detachment from the tip of different capillary tubes in quiescent water were tested. The aim was to provide an accurate cross-calibration of two of the methods against a standard laboratory method. The inverted funnel method is the laboratory standard and performed within a 0.5% repeatability error for 50 bubble sets. The passive acoustic method performed within an accuracy between 97% and 99% with respect to the inverted funnel method. The photographic method gave an accuracy between 88% and 96%. After improvement of the photographic method by an empirical cutting edge criterion, its accuracy was raised between 95% and 99%. The bubble shape at detachment was found to be fitted by a Cassini's oval or by a Bernoulli's lemniscate according to the formation time. Qualitative observations on the bubble formation stage indicated an early vertical nose growth for the larger diameter capillary tubes at short formation times. The major-axis vertical and horizontal lengths were measured as functions of time at the formation stage.

Keywords: Bubble generators; Bubble size measurement; Passive acoustic; Inverted funnel; Visualization techniques

1. Introduction

Gas–liquid bubble flow is essential in a great number of industrial processes such as biochemical processes: glucose–gluconic acid biotransformation [1], fermentation in bioreactors [2], biological wastewater treatment [3]; and other chemical processes [4–6]. Gas–liquid flows also occur in the natural environment, such as in geophysics [7–11] and aerosol dynamics [12]. In spite of the simple design of industrial equipment, the behavior of bubbles is complicated and difficult to predict.

Understanding the behavior of a single bubble can support a better knowledge of the overall behavior and has been the subject of many studies [13–19]. Besides, it is widely known that the bubble diameter and its motion affect the design of mass transfer equipment [20,21]. The gas injector design is meaningful in the determination of bubbling regimes and their evolution, the bubble diameter and motion can be studied experimentally with high quality results where there is only one bubble. However, the bubbles are generated by porous ceramic stones and pipes or plates with multiple orifices (spargers), flexible membranes, agitated tanks or capillary tubes, and of course, complex bubbly flows can result with multiple scales of motion and bubble size.

The need to understand complex bubbly flows has inspired the development of numerous techniques over the last decade that can also specify the shape and volume of bubbles with improved accuracy and high-speed. Such methods are useful in practical complex flows, or at least have the potential to be useful. However, there

* Corresponding author. Fax: +52 55 5804 4900.
E-mail address: asor@xanum.uam.mx (A. Soria).

0894-1777/$ - see front matter © 2005 Elsevier Inc. All rights reserved.
doi:10.1016/j.expthermflusci.2005.03.018

is no calibration standard for them. The most used methods are: high-speed photography [22–27]; electrical impedance tomography [28], capillary suction probes [20], optical waveguided sensors [29,30]; endoscopic optical probes [31,32]; capacitance probes [23] and passive acoustic detection [14,15,33]. There are some disagreements among them, since some offer greater rapidity of detection but are constrained by the sensing element sensitivity or by data interpretation issues (passive acoustic, capacitance and electric impedance methods), while others depend on the purity of the liquid medium and lighting effects (photographic and optical methods). In fact, the lighting may produce a play of several reflections and refractions. These should be considered in order to determine a threshold level for the bubble size estimation, since some reflections on the frontal part of the bubble may reduce the apparent bubble size [22,34].

Although many studies on bubble size have been made using these various methods, there are only a few systematic studies comparing optical and acoustic methods, such as Longuet-Higginns et al. [35], Manasseh [36], Manasseh et al. [15] and Zhu et al. [32]. Moreover, no published studies so far have determined the relative accuracy of the methods against a calibration standard for precisely-formed, single bubbles. In order for acoustic and optical bubble-sizing methods to be applied in complex bubbly flows, an accurate cross-calibration of these techniques against a laboratory standard is required.

In this paper we obtain the size of single air bubbles in a viscous Newtonian fluid (water) in an effectively unbounded domain by three methods: the photographic, the acoustic and the inverted funnel. We took as a laboratory-standard reference the results obtained by the inverted funnel method, also known as the capillary suction probe. This method is the most accurate since the bubble size is computed from the direct volume quantification. For the acoustic technique, a commercial piezoelectric element with a lower sensitivity than that of a conventional hydrophone (e.g. the Bruel and Kjaer type 8103) was used. For the photographic method, a high-speed video camera (Motion Scope System 8000S, MASD-Red Lake Inc.) was used. In order to find the bubble size, the bubble shape was fitted by a Bernoulli's lemniscate or by a Cassini's oval function. We also observed the development of a nose at the bubble top at an early stage of the bubble formation. The vertical (a) and horizontal (b) major-axis lengths in this generation process were measured as they evolved in time. With these purposes, the paper is organized as follows: In Section 2 we describe the experimental set-up, we discuss the main experimental methods from the literature and how the experiments took place. In Section 3, we discuss our results and finally, we conclude, pointing out some advantages, limitations and possible generalizations of the various methods.

2. Experimental set-up and procedures

This chapter for experimental set-up is divided into the experimental tank and bubble generators, the measuring techniques and the procedure.

2.1. Experimental tank and bubble generators

The experiments were done in a rectangular glass tank $0.80 \times 0.80 \times 0.60$ m and 0.006 m in wall thickness, large enough to neglect the wall effects [37]. The bubbles were generated at 0.506 ± 0.006 m below the liquid level. Fig. 1 shows the schematic experimental apparatus. The temperature in the tank for the experimental runs was $T = 24 \pm 0.5$ °C; the water density $\rho = 997$ kg/m^3 (balance hydrometer), the viscosity $\mu = 0.900 \times 10^{-3}$ kg/(m/s) (Ostwald viscometer) and the surface tension $\sigma = 72.80 \times 10^{-3}$ N/m (Fisher tensiometer). Single bubbles were generated at the bottom center line of the tank, using a specially-designed L-shape adaptor, 0.0012 m inner diameter and 1.12 m length (see Fig. 1), connecting the electronic valve to microcap capillary tubes (Drummond Scientific Company) with flat tops. Four capillary tubes with internal diameters ranging from 0.39×10^{-3} to 0.99×10^{-3} m $\pm 1\%$ were used. Air was supplied with a regulated pressure pump, filtered and saturated with water in a globe flask in order to avoid the bubble volume changes produced by water absorption [38]. An usually closed micro-electronic valve (PSV-1, Aalborg Instruments and Controls Inc.), was opened at a given time and an air pulse was sent through the pipe, connecting the globe flask to the air circuit, up to the needle where the bubble was formed and detached. The pressure up-stream the valve was measured by a manometer (Metron Instruments, $0–43.09 \times 10^2$ N/m^2), before a pulse was produced. Bubbles were generated in the stagnant liquid every 3 min in order to allow the liquid motion induced by the previous bubble to be damped, and avoiding hydrodynamic interactions other than those due to the isolated bubble motion.

2.2. Measuring techniques

2.2.1. Video imaging

Bubble generation was recorded with a high-speed video camera (Motion System 8000S, MASD-Red Lake Inc.) at 4000 frames per second. The camera was operated in the full frame mode which had a resolution of 100×98 pixels. An optical array made of a Precise Eye lens (1-61453) with less than 0.14% distortion and a Biconvex KB7 lens with 100 mm focal length were used, giving one pixel per 9.6×10^{-3} mm. The images were digitized directly from the cameras. Illumination was provided by a 500 W halogen lamp which illuminated the rear container wall. Radiation from the lamp was tested to be negligible by temperature measurements

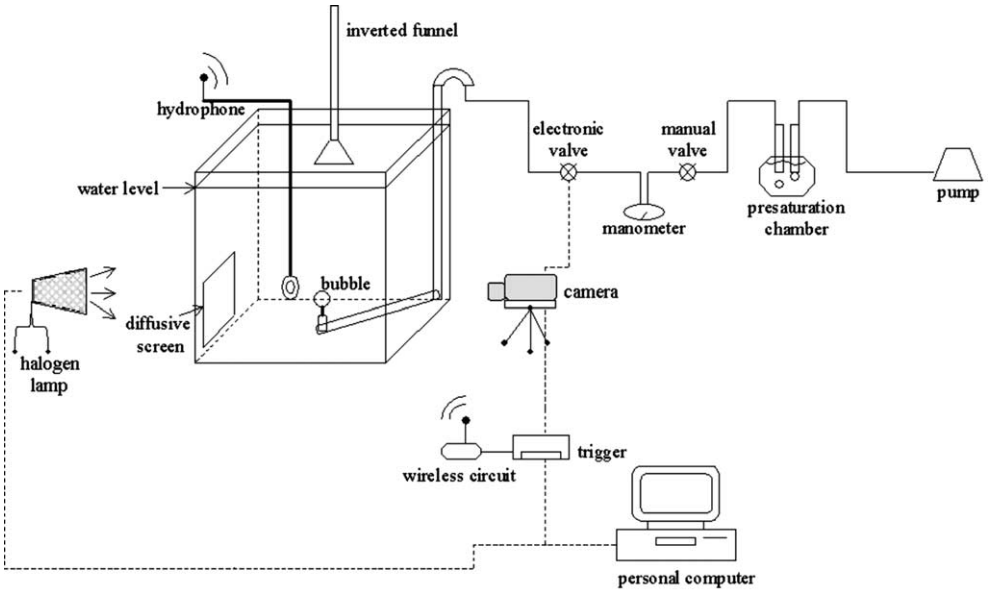

Fig. 1. Sketch of the experimental set-up.

inside the tank. The opposite wall was covered with a diffusion screen to avoid undesired reflections and refractions as much as possible. The experiment took place when the electronic valve was activated, triggering both capture systems: the video camera and the hydrophone, in a computer-controlled environment.

2.2.2. Acoustic sensor

The acoustic method was introduced by Minnaert [39], who related the bubble detachment from a nozzle to its acoustic signal. In this analysis, the bubble volumetric vibration at small amplitudes was approximated by the classical simple harmonic oscillator. Neglecting surface tension as well as dissipation effects and assuming adiabatic conditions, the Minnaert resonance frequency is given by

$$v = \frac{1}{2\pi r_{\mathrm{equ}}^{\mathrm{A}}}\sqrt{\frac{3\gamma P}{\rho}} \tag{1}$$

where v is the frequency in Hz, γ is the ratio of specific heats for the gas, ρ is the liquid density, P is the absolute liquid pressure, and $r_{\mathrm{equ}}^{\mathrm{A}}$ is the bubble radius. It can be shown that surface tension corresponds to a second-order effect [35]. This method was fully reviewed by Leighton [40] for spherical bubbles, and it has been applied successfully in engineering equipment such as aeration systems [15,41]. It has also been used for monitoring the equipment status and the physical and chemical changes in different processes at real time [42]. Its great advantages are low cost and reliability. Moreover, since the devices used as transducers (hydrophones) are made of piezoelectric materials, this technique is independent of fluid properties.

In this work, a piezoelectric element (Radio Shack Co., #273-0073) was adapted to be used as a hydrophone and placed inside an aluminum holding tube with a diameter of 0.0205 ± 0.005 m and 0.52 ± 0.005 m length. This element was connected to a wireless microphone in order to amplify and convert the electric signal into an acoustic one. The use of a wireless transducer also offers a practical advantage, since industrial measurements in some inaccessible geometries could be made remotely. The latter was captured with an audio card (Sound Blaster 64 PCI) and analyzed with Cool Edit Pro software 2.0 (Syntrillium Corp.). Following Manasseh et al. [15], the hydrophone was located 0.05 m away from the bubble generator in order to minimize the perturbation on the bubble dynamics and to maximize the quality of the acoustic signal as much as possible. Testing acoustic signals showed the tank was sufficiently large to neglect reverberation. The hydrophone detected the bubble sound at detachment. The bubble size was obtained by analyzing the acoustic signal for the first five cycles with a fast Fourier transform (Fig. 2). We obtained the dominant frequencies in the range of 1–2 kHz, as expected from Eq. (1).

Although commercial hydrophones (e.g. Bruel and Kjaer type 8103), have linear frequency responses in the 1–10 kHz band, the piezoelectric element frequency response used in our experiments exhibited a non-linear behavior, as can be seen in Fig. 3 where a variable sound pressure dependent upon the frequency is apparent. In addition, the novel combination of a piezoelectric element and wireless microphone, while offering many practical advantages, appeared to saturate in amplitude rather than displaying the classical exponentially-decaying acoustic pulse observed by many authors

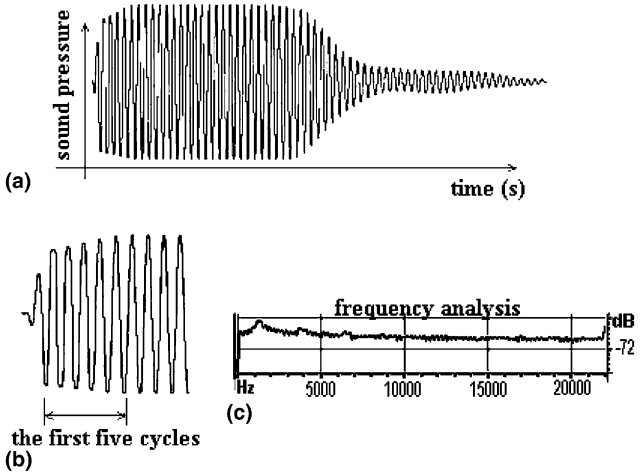

Fig. 2. Acoustic procedure: (a) acoustic signal, (b) sequence of five cycles and (c) dominant frequency.

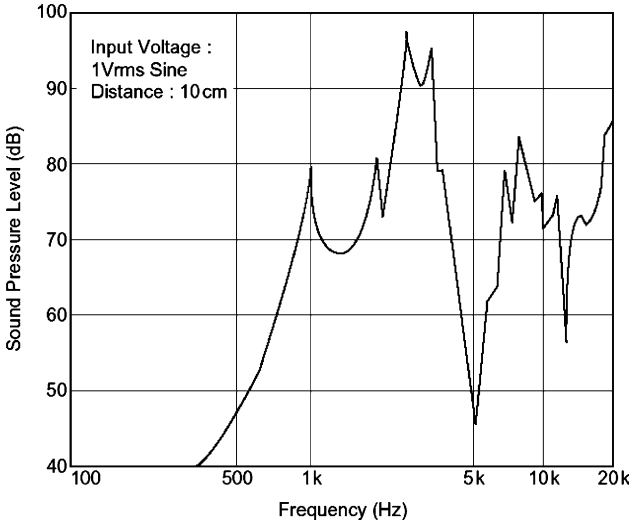

Fig. 3. Typical receiving frequency characteristics of piezoelectric element.

[35,40,43]. However, the only relevant parameter to Minnaert's expression is the frequency and therefore, the sound pressure changes are irrelevant to the bubble size measurements provided there is only one bubble at a time [15,44].

2.2.3. Inverted funnel

Another way to measure the bubble diameter is the inverted funnel method, described in detail by Leighton and Walton [43]. The bubble is trapped in an inverted cone and induced into a capillary tube where the length of the air column is measured. In this paper, bubbles were caught by an inverted pyrex-glass funnel (KIMBLE/KONTES) with 58° cone angle. The funnel was connected to an internal radius 0.42 ± 0.01 mm capillary tube provided with a graduated scale. A syringe at the tube top sucked the air bubble into the capillary tube. The bubble volume was then estimated from the air bridge inside the capillary tube. Considering the air as an ideal gas, the bubble size was corrected for pressure and surface tension effects, giving a 6% of bubble volume change.

2.3. Procedure

A triggering circuit (TI-01 HIQUEL timer) was adapted for synchronizing the camera, the PS-1 valve and the hydrophone. In this way each individual bubble was recorded by both the video system and the hydrophone and then collected by the inverted funnel. The volumes and the bubble growth curves were evaluated by video image analysis, using IMAQ Vision Builder 6.1 Software (National Instruments Corp.).

3. Results and discussion

3.1. Sizes

We studied the bubble shape and size at detachment for four inner diameter (ϕ) capillary tubes, as shown in Fig. 4. The origin of the time axis in Fig. 4 was selected as the time of the bubble detachment. The bubble detachment time ($t = 0$) was taken as half the interval between the last frame where the bubble is in contact with the capillary tube and the first frame where the bubble is separated from the capillary tip (called the detachment frame). In this way, the actual detachment time is coincident with our definition, with an uncertainty bound equal to ±0.125 ms.

Two evolution patterns for bubbles detaching from the 0.99 mm inner diameter capillary tip are shown in Fig. 4. The bubble sizes and shapes at detachment for

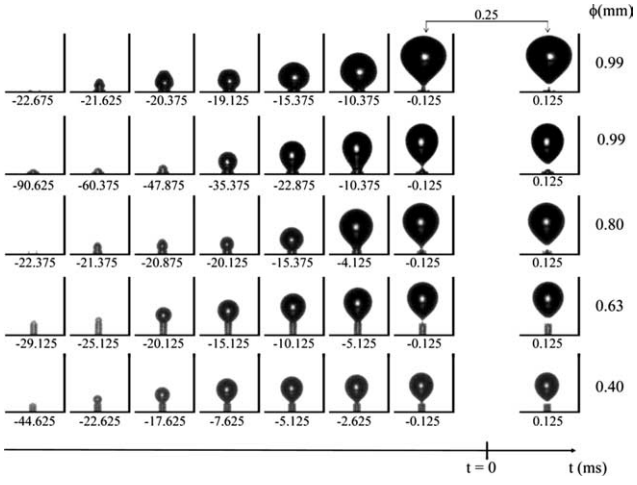

Fig. 4. Bubble formation and detachment at the tip of capillary tubes for four inner diameters.

both patterns are different and seem to be dependent upon the elapsed time taken for the bubble to form at the capillary tip. Small variations in the initial upstream pressure at the capillary tip may be found responsible for the different detachment shapes. These variations could be appreciated by the size of a liquid plug inside the capillary tip at the beginning of the experiment. The length of this liquid plug changed between 0.002 and 0.012 m. In this discussion two data sets for bubbles detached at the 0.99 mm inner diameter capillary tip are shown, each one corresponding to a 50-bubbles sample set with a specific bubble shape and size.

The calculation of bubble volume from images of arbitrarily distorted bubbles has been studied by Lunde and Perkins [22] and Zhu et al. [32] (and references therein). We performed three procedures on the photographic method for the evaluation of the bubble size at detachment. As a first procedure, (Photographic Method I) the values of the vertical (a) and horizontal (b) major-axis lengths were obtained for each bubble, with the so-called Advanced Edge Detection algorithm (from the IMAQ Vision Builder). In this algorithm the bubble edge is defined as the locus where the maximum difference in grey tone values between adjacent pixels is obtained. Mean values for the 50 bubble sets were then evaluated and the mean equivalent radius, defined as $r_{\mathrm{equ}}^{\mathrm{P1}} = \sqrt{ab}$ was also computed. A second procedure (Photographic Method II), for bubble size estimation at detachment, was done by fitting a Bernoulli's lemniscate or a Cassini's oval, according to the observed shape, as could be seen in the detachment frame ($t = 0.125$ ms) in Fig. 4. Of course, the lemniscate and the oval functions presume the bubble is axisymmetric, which is clearly the case at formation in quiescent liquid. However, analogous contour-measurement methods, e.g. that of Lunde and Perkins [22] may be applicable in more general bubbly flows. The present analysis is intended to quantify the error inherent in the optical method, presuming the best available contour measurement is used. We selected the best edge fitting to one of the mentioned curves (Fig. 5), by substituting the measured horizontal (b) and vertical (a) axes in the analytical expressions, given by

$$\text{Bernoulli's lemniscate} \quad r = [\cos(2\theta) \times 10^4]^{9/50} \tag{2}$$

$$\text{Cassini's oval} \quad r = \pm a \times \sqrt{\left[\cos(2\theta) \pm \sqrt{\left(\frac{b}{a}\right)^4 - \sin^2(2\theta)}\right]} \tag{3}$$

where

$$\theta = \arctan\left(\frac{b}{a}\right)$$

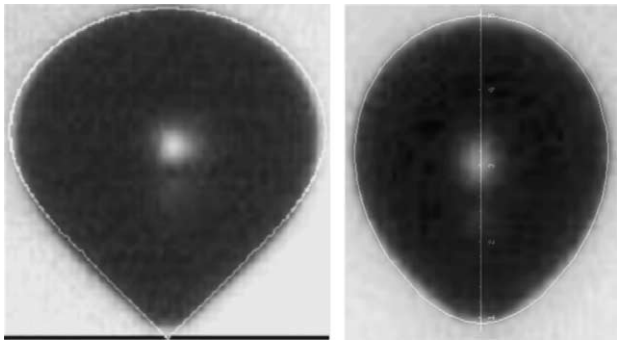

Fig. 5. Bubble edge perimeter fitting (white line embodying the bubble) to a Bernoulli's lemniscate and to a Cassini's oval, respectively.

An equivalent radius, $r_{\mathrm{equ}}^{\mathrm{P2}}$, was found from the volume, V, obtained by the best fit integration of the solid of revolution around the major axis, according to the expression

$$r_{\mathrm{equ}}^{\mathrm{P2}} = \left(\frac{3V}{4\pi}\right)^{\frac{1}{3}} \tag{4}$$

The third bubble size estimation procedure for the photographic method (Photographic Method III) begins with the superposition of the 50 images in a set, in order to get a smoothed image with a better edge definition. The bubble edge is defined with the so called, Clustering Threshold algorithm from the IMAQ Vision Builder. After a multi-clustering process, two mean grey values are obtained, identifying the bubble and its surroundings. The bubble edge is defined as the locus of grey level equal to the average of the mean values. After superposition of the images, the a and b axes are obtained in the resulting picture, the bubble volume is evaluated considering the bubble shape and finally the equivalent bubble radius is evaluated from Eq. (4).

Fifty bubbles from each capillary tube were analyzed by the three methods to generate statistically meaningful equivalent bubble radii, r_{equ}, as well as their corresponding standard deviations. Furthermore, to quantify the differences between the acoustic and the photographic methods on one hand and the inverted-funnel method on the other, an accuracy definition was introduced as

$$A \equiv 1 - \frac{\left|r_{\mathrm{equ}}^{\mathrm{IF}} - r_{\mathrm{equ}}^{i}\right|}{r_{\mathrm{equ}}^{\mathrm{IF}}} \tag{5}$$

Here the superscript IF is for the inverted funnel method, and the superscript i indicates the acoustic or the photographic method. In Table 1, the resulting equivalent radius and its accuracy for the three methods are shown.

In Table 1 it can be observed that the Photographic Method I performs with an accuracy from 86% to 99% with respect to the inverted funnel. The Photographic Method I performs with the best accuracy (around

Table 1
Bubble mean radius and its accuracy for the three methods

Capillary diameter, ϕ (mm)	Bubble mean radius (mm)								
	Inverted funnel method ±0.5%	Photographic Method I ±5%		Photographic Method II ±1%		Photographic Method III ±1%		Passive acoustic method ±0.3%	
	r_{equ}^{IF}	r_{equ}^{P}	A	r_{equ}^{P}	A	$r_{equ}^{P'}$	A	r_{equ}^{A}	A
0.99	2.45	2.44	0.99	2.30	0.94	2.21	0.90	2.36	0.97
0.99	1.94	1.92	0.99	1.69	0.88	1.98	0.98	1.92	0.99
0.79	1.97	2.24	0.86	1.81	0.92	1.85	0.94	1.99	0.98
0.63	1.82	1.86	0.98	1.73	0.96	1.74	0.96	1.80	0.99
0.39	1.39	1.41	0.99	1.31	0.95	1.28	0.92	1.39	0.99

Each statistics calculated for 50 bubbles.

0.99); however, it should be stressed that the worst accuracy also occurred under Photographic Method I, for the 0.79 mm inner diameter capillary tube. Moreover, the repeatability of this procedure was within 5%. The Photographic Methods II and III performed better than Photographic Method I in their repeatability, which was around 1%. Nevertheless, as noted, Methods II and III had lower accuracies than Method I, varying from 0.88 to 0.96 for Method II and from 0.90 to 0.98 for Method III.

The passive acoustic method, on the other hand, performed well in both, accuracy and repeatability, since its repeatability was 0.3% and its accuracy range between 0.97 and 0.99. This suggests that the piezoelectric element performs well for these bubble sizes.

In Fig. 6 the bubble size measured by all the three methods is shown, illustrating the bubble radius underestimation by the photographic method. This result should be understood as due to the introduction of reflections at the bubble surface, which cause an obscuration of the actual bubble edge and thus a bias in the measured size.

Recent investigations by Leifer et al. [45] indicate that off-axis external reflections cause a bright ring which obscures the true bubble edge. Neglecting this effect, particularly if an inappropriate threshold is used, may cause bubble size underprediction as large as 10–15%. They also mention that the appropriate threshold is slightly below the local background intensity. It was following these observations and those of Nomura and Naruse [46], who considered stationary-scene multiple images to reduce random obscuring or drop-out noise, that we developed the Photographic Method III. In Fig. 7 the bubble size evaluated by the three photographic methods are shown, together with the inverted funnel results for comparison.

3.2. Growth

Although the focus of the present paper is the comparison of experimental methods, owing to the comprehensive measurements made, we are also able to report very detailed observations of the bubble growth at the capillary. We measured the vertical (a) and the horizon-

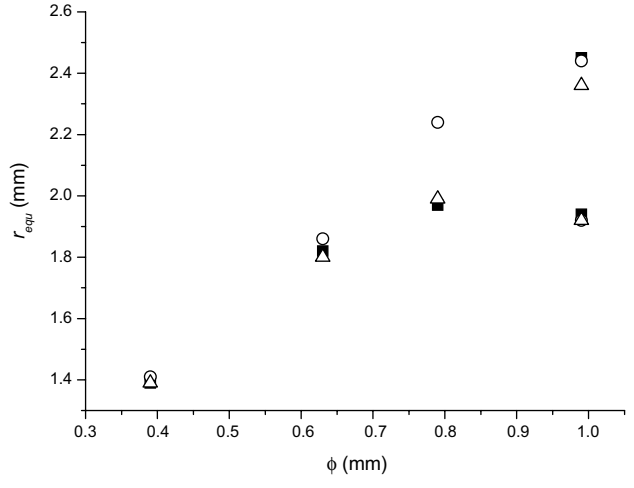

Fig. 6. Bubble size measured with (■) inverted funnel, (○) Photographic I and (△) acoustic methods.

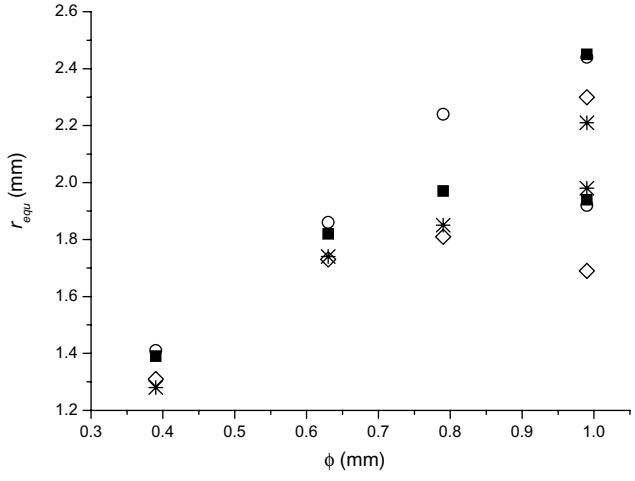

Fig. 7. Bubble size measured by photographic methods and the (■) inverted funnel as a reference. (○) Photographic Method I, (◇) Photographic Method II and (✳) Photographic Method III.

tal (b) major-axis lengths during the formation stage. Different growth patterns for lemnisca-shaped bubbles and for oval bubbles are apparent (see Figs. 8 and 9). The beginning of the formation process was taken as the first time when one or both axes increased its initial slope. This definition was convenient since an incipient stagnant gas meniscus was observed at the tip for some capillary tubes, before the growth process started. The initial horizontal length was found greater than the vertical length when the stagnant gas meniscus was observed (Figs. 8 and 9). On the other hand, when no stagnant gas meniscus was observed, both initial lengths were found to vanish (Fig. 9). While the oval bubbles' formation time was found dependent on the gas flow rate, it seemed to be independent and close to 23 ms for lemnisca-shaped bubbles.

The initial vertical growth rate was found greater than the horizontal one for oval bubbles (Fig. 8), tending to a nearly spherical shape, crossing over to an elongated shape with a greater vertical axis, and continuing up to detachment.

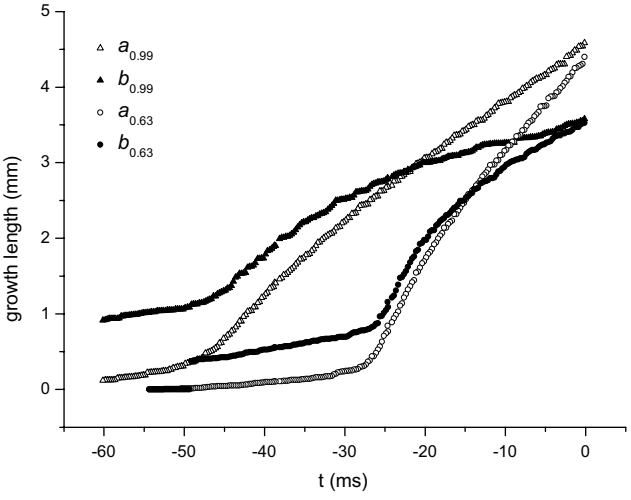

Fig. 8. Growth length for oval bubbles.

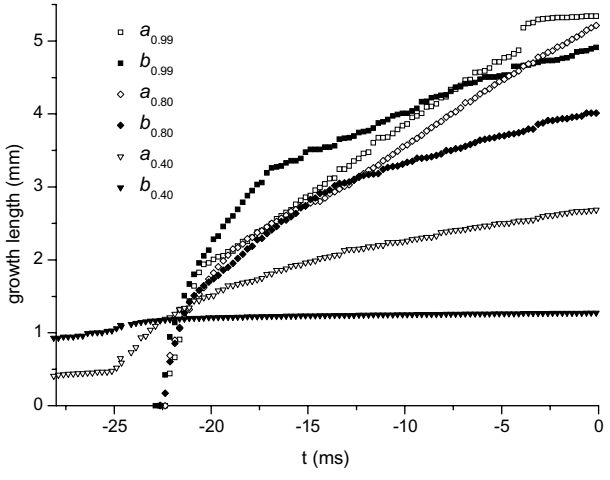

Fig. 9. Growth length for lemnisca-shaped bubbles.

For lemnisca-shaped bubbles (Fig. 9), the initial growth of the vertical and the horizontal axes were found similar, when no stagnant gas meniscus was present at the beginning. However, the bubble shape was not close to spherical, with a nose formation apparent at its top. The behavior of this nose could be observed for the largest diameter capillary tube, where a subsequent retardation in vertical growth was found, followed by a constant growth rate. Meanwhile the horizontal axis continued its growth, forming the typical lemniscate length (greater than the typical oval horizontal length). A further crossover of both axes was noted close to detachment.

4. Conclusions

Two measurement methods for determining the volume and the equivalent radius of air bubbles were evaluated. This analysis was made by comparison with a third, the laboratory-standard inverted-funnel method, at bubble detachment in a quiescent fluid (water). The inverted funnel method performed within a 0.5% repeatability error for a 50-bubble set and was taken as a reference for comparison with the other methods due to its reliability [40]. A first evaluation of the photographic method, which included our use of analytic functions to fit the bubble profile, gave accuracy between 86% and 99% within a 5% repeatability error. Several possible error and bias sources were pointed out, one due to the lighting reflections and refractions which could confuse the bubble-edge image with the background, causing a bias in the size estimation. We selected an image superposition method in order to improve the edge definition criterion, which together with an equivalent radius estimation based on the volume evaluation considering the true bubble shape, gave improved bubble size estimation with accuracy between 90% and 98% within a 1% repeatability error. While the most recent improvements on the photographic method are simply based on a technique of superposing the whole set of data, further improvements should have as its theoretical foundation an analysis of light scattering. The bubble shape at detachment was found to be fitted by a Cassini's oval or by a Bernoulli's lemniscate, depending on the formation time. The bubble growth at the capillary tip was followed during the formation stage and its evolution was qualitatively characterized. In more complex bubbly flows, the bubbles would not necessarily be axisymmetric and the photographic method seems to be the only one that can measure non-spherical bubbles accurately, when the actual bubble shape is desired. Moreover, if the bubble volume is the only important size variable, the acoustic method should be

preferred, since acoustic data may be processed easily and faster than image processing. Also in dark or turbid media, the acoustic method is available, while the photographic method is not.

The second measurement method evaluated was passive acoustics, which performed with accuracy between 97% and 99% and a repeatability of 0.3%, suggesting the piezoelectric element performed appropriately for bubbles from 1.39 mm to 2.45 mm equivalent bubble radius.

In conclusion, the improved optical method shows promise for detailed laboratory studies of bubble formation processes, yielding accurate data on bubble shapes as well as sizes. An optical method with good contour-fitting could possibly also be used for laboratory studies of turbulent bubbly flows, provided access for imaging is possible. The acoustic method was demonstrated to be equally accurate, and moreover, feasible using a piezoelectric element instead of a conventional hydrophone. This offers a major cost-saving, potentially making the passive acoustic technique of widespread industrial relevance with inexpensive equipment. It is applicable to a very wide variety of practical industrial and laboratory systems.

Acknowledgments

The authors gratefully acknowledge Prof. Ira Leifer for useful advice and comments and the Universidad Autónoma Metropolitana for financial support.

References

[1] J. Klein, M. Rosenberg, J. Markoš, O. Dolgoš, M. Krošlák, L. Krištofíková, Biotransformation of glucose to gluconic acid by *Aspergillus niger*—study of mass transfer in an airlift bioreactor, Biochem. Eng. J. 10 (2002) 197–205.

[2] N.A. Mensour, A. Margaritis, C.L. Briens, H. Pikington, I. Russell, New developments in the brewing industry using immovilized yeast cell bioreactor systems, J. Inst. Brew. 103 (1997) 363–370.

[3] A. Prakash, A. Margaritis, R.C. Sauders, S. Vijayan, High concentrations ammonia removal by the cyanobacterium plectonema boryanum in a photobioreactor system, Can. J. Chem. Eng. 77 (1999) 99–107.

[4] J.R. Boles, J.F. Clark, I. Leifer, L. Washburn, Temporal Variation in natural methane seep rate due to tides, coil oil point area, California, J. Geophys. Res. 106C11 (2000) 27077–27086.

[5] J. Magnaudet, I. Eames, The motion of high-Reynolds number bubbles in inhomogeneous flows, Annu. Rev. Fluid Mech. 32 (2000) 659–668.

[6] R. Clift, J.R. Grace, M.E. Weber, Bubbles, Drops and Particles, Academic Press, New York, 1978.

[7] W.E. Asher, L.M. Karle, B.J. Higgins, P.J. Farley, I. Leifer, E.C. Manahan, The influence of bubble plumes on air–seawater gas transfer velocities, J. Geophys. Res. 101C (1996) 1207–12041.

[8] I. Leifer, R. Patro R, The bubble mechanism for transport of methane from the shallow sea bed to the surface: a review and sensitivity study, Continental Shelf Res. 22 (16) (2002) 2409–2428.

[9] H. Medwin, N.D. Breitz, Ambient and transient bubble spectral densities in quiescent seas and under spilling breakers, J. Geophys. Res. 94C (1989) 12571–12759.

[10] S. Vergniolle, G. Brandeis, Strombolian explosions 1. A large bubble breaking at the surface of a lava column as a source of sound, J. Geophys. Res. 101 (B9) (1996) 20433–20447.

[11] S. Vergniolle, G. Brandeis, J.C. Mareschal, Strombolian explosions 2. Eruption dynamics determined from acoustic measurements, J. Geophys. Res. 101 (B9) (1996) 20449–20466.

[12] S.K. Friedlander, Smoke, Dust, and Haze, Oxford University Press, New York, 2000.

[13] P.C. Duineveld, The rise velocity and shape of bubbles in pure water at high Reynolds number, J. Fluid Mech. 292 (1995) 325–332.

[14] R. Manasseh, Y. Yoshida, M. Rudman, Bubble formation processes and bubble acoustic signals, in: Third International Conference on Multiphase Flow, Lyon, France, June 1998, p. 426.

[15] R. Manasseh, R.F. La Fontaine, J. Davy, I. Sheperd, Y.G. Zhu, Passive acoustic bubble sizing in sparged systems, Exp. Fluids 30 (6) (2001) 672–682.

[16] T. Maxworthy, C. Gnann, M. Kürten, F. Durst, Experiments on the rise of air bubbles in clean viscous liquids, J. Fluid Mech. 321 (1996) 421–441.

[17] A. Biesheuvel, L. van Wijngaarden, Two-phase of equations for a dilute dispersion of gas bubbles in liquid, J. Fluid Mech. 148 (1998) 301–318.

[18] H. Oğuz, A. Prosperetti, Dynamics of bubble growth and detachment from a needle, J. Fluid Mech. 257 (1993) 11–145.

[19] A.W.G. de Vries, A. Biesheuvel, L. van Wijngaarden, Notes on the path and wake of a gas bubble rising in pure water, Int. J. Multiphase Flow 28 (2002) 1823–1835.

[20] M. Barigou, M. Greaves, A capillary suction probe for bubble size measurement, Meas. Sci. Technol. 2 (1991) 318–326.

[21] F.J. Montes, M.A. Galan, R.L. Cerro, Comparison of theoretical and experimental characteristics of oscillating bubbles, Ind. Eng. Chem. Res. 41 (2002) 6235–6245.

[22] K. Lunde, R.J. Perkins, A method for the detailed study of bubble motion and deformation, in: A. Serizawa, T. Fukano, J. Bataille (Eds.), Proc. Int. Conf. Multiphase Flow, Multiphase Flow 1995, Elsevier Science B.V., Amsterdam, 1995, pp. 395–405.

[23] I. Leifer, G. De Leeuw, L.H. Cohen, Optical measurement of bubbles: System, design and application, J. Atmos. Oceanic Technol. 17 (10) (2000) 1392–1402.

[24] M. Wu, M. Gharib, Contamination is not the only way to slow down rising air bubbles, in: American Physical Society 53rd Annual Meeting of the Division of Fluid Dynamics, Washington DC, 2000.

[25] M. Wu, M. Gharib, Experimental studies on the shape and path of small air bubbles rising in clean water, Phys. Fluids 14 (2002) L49–L52.

[26] K. Ellingsen, F. Risso, On the rise of an ellipsoidal bubble in water: Oscillatory paths and liquid-induced velocity, J. Fluid Mech. 440 (2001) 235–268.

[27] S.S. Alves, C.I. Maia, J.M.T. Vasconcelos, A.J. Serralheiro, Bubble size in aerated stirred tanks, Chem. Eng. Sci. 89 (2002) 109–117.

[28] M.C. Kim, S. Kim, H.J. Lee, Y.J. Lee, K.Y. Kim, An experimental study of electrical impedance tomography for the two-phase flow visualization, Int. Commun. Heat Mass Transfer 29 (2002) 193–202.

[29] B. Saberi, K. Shakourzadeh, J. Militzer, Application of fiber optic probe to the hydrodynamic study of an industrial fluidized bed furnace, Proc. Int. Conf. Fluid Bed Combust. 14 (1997) 595–601.

[30] M.R. Rząsa, A. Pląskowski, Application of optical tomography for measurement of aereation parameters in large water tanks, Meas. Sci. Technol. 14 (2003) 199–204.

[31] J. Chabot, S.L.P. Lee, A. Soria, H.I. de Lasa, Interaction between bubbles and fiber optic probes in a bubble column, Can. J. Chem. Eng. 70 (1991) 61–68.
[32] Y. Zhu, J. Wu, R. Manasseh, Rapid measurement of bubble size in gas–liquid flows using a bubble detection technique, in: Proc. 14th Australasian Fluid Mechanics Conference, Adelaide University, Adelaide, Australia, 10–14 December 2001.
[33] H. Chanson, R. Manasseh, Air entrainment processes in a circular plunging jet: Void-fraction and acoustic measurements, J. Fluids Eng. Trans. ASME 125 (2003) 910–921.
[34] C. Bongiovanni, A. Dominguez, J.P. Chevaillier, Understanding images of bubbles, Eur. J. Phys. 21 (2000) 561–570.
[35] M.S. Longuet-Higginns, B.R. Kerman, K. Lunde, The release of air bubbles from an underwater nozzle, J. Fluid Mech. 230 (1991) 365–390.
[36] R. Manasseh, Acoustic sizing of bubbles at moderate to high bubbling rates, in: M. Giot, F. Mayinger, G.P. Celata (Eds.), Experimental Heat Transfer, Fluid Mechanics and Thermodynamics, Edizioni ETS, Pisa, 1997, pp. 943–947.
[37] V. Filderis, R.L. Whitmore, Experimental determination of the wall effect for spheres falling axially in cylindrical vessels, Br. J. Appl. Phys. 12 (1961) 490–497.
[38] D. Manley, Change of size of air bubbles in water containing a small dissolved air content, Br. J. Appl. Phys. 11 (1960) 38–42.
[39] M. Minnaert, On musical air-bubbles and sounds of running water, Phil. Mag. 16 (1933) 235–248.
[40] T.G. Leighton, The Acoustic Bubble, Academic Press, Cambridge, UK, 1994.
[41] R. Manasseh, Passive acoustic analysis of complex bubbly flows, in: 16th International Congress of Chemical and Process Engineering, Prague, Czech Republic, 22–16 August 2004.
[42] J.W.R. Boyd, J. Varley, The uses of passive measurement of acoustic emissions from chemical engineering processes, Chem. Eng. Sci. 56 (2001) 1749–1767.
[43] T.G. Leighton, A.J. Walton, An experimental study of the sound emitted from gas bubbles in a liquid, Eur. J. Phys. 8 (1987) 98–104.
[44] R. Manasseh, A. Nikolovska, A. Ooi, S. Yoshida, Anisotropy in the sound field generated by a bubble chain, J. Sound Vib. 278 (4–5) (2004) 807–823.
[45] I. Leifer, G. De Leeuw, G. Kunz, L.H. Cohen, Calibrating optical bubble size by the displaced-mass method, Chem. Eng. Sci. 58 (2003) 5211–5216.
[46] Y. Nomura, H. Naruse, Reduction of obscuration noise using multiple images, Pattern Anal. Machine Intell., IEEE Trans. 10 (1988) 267–270.